

IML-ViT: Benchmarking Image Manipulation Localization by Vision Transformer

Xiaochen Ma¹, Bo Du¹, Zhuohang Jiang¹, Ahmed Y. Al Hammadi², and Jizhe Zhou¹

¹ Sichuan University

² Mohamed Bin Zayed University for Humanities

Abstract

Advanced image tampering techniques are increasingly challenging the trustworthiness of multimedia, leading to the development of Image Manipulation Localization (IML). But what makes a good IML model? The answer lies in the way to capture artifacts. Exploiting artifacts requires the model to extract non-semantic discrepancies between manipulated and authentic regions, necessitating explicit comparisons between the two areas. With the self-attention mechanism, naturally, the Transformer should be a better candidate to capture artifacts. However, due to limited datasets, there is currently no pure ViT-based approach for IML to serve as a benchmark, and CNNs dominate the entire task. Nevertheless, CNNs suffer from weak long-range and non-semantic modeling. To bridge this gap, based on the fact that artifacts are sensitive to image resolution, amplified under multi-scale features, and massive at the manipulation border, we formulate the answer to the former question as building a ViT with high-resolution capacity, multi-scale feature extraction capability, and manipulation edge supervision that could converge with a small amount of data. We term this simple but effective ViT paradigm IML-ViT, which has significant potential to become a new benchmark for IML. Extensive experiments on five benchmark datasets verified our model outperforms the state-of-the-art manipulation localization methods. Code and models are available at <https://github.com/SunnyHaze/IML-ViT>

1. Introduction

As multimedia editing technology advances, we increasingly need advanced Image Manipulation Localization (IML) methods to cope with existing tampered images and avoid security threats [27]. As shown in Figure 1, this task aims to detect whether images have been modified and to localize the modified regions at the pixel level in a segmentation manner. Image manipulation can be generally classified into three types [30, 27]: (1) *splicing*: copying

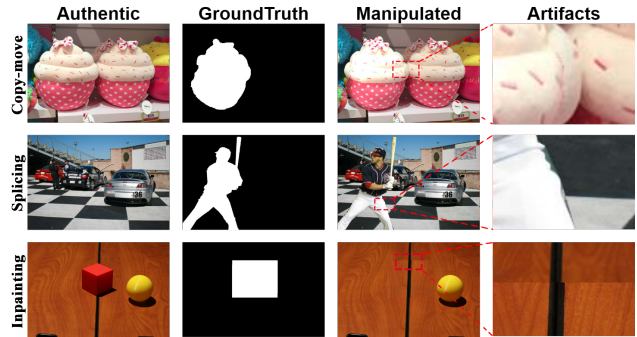


Figure 1: **An example of three types of manipulations and their corresponding visible artifacts.** Visible traces include distortions, sudden changes, or anomalies caused by tampering operations, which are frequently found at the junction between two regions and appear in very detailed positions. For a better view, zooming in is recommended.

a region from an image and pasting it to another image. (2) *copy-move*: cloning a region within an image. (3) *inpainting*: erasing regions from images and inpaint missing regions with visually plausible contents.

As shown in Table 1, most existing methods for IML tasks greatly benefit from tracing artifacts with various CNN-based feature extractors. “Artifacts” refer to unique visible traces (as shown in Figure 1) and invisible low-level feature inconsistencies (e.g., noise or high-frequency) resulting from manipulation. As tampering aims to deceive the audience by creating semantically meaningful and perceptually convincing images, visual traces typically manifest at a non-semantic level, distributed in textures around the manipulated area. Additionally, low-level features, like noise inconsistencies introduced by different cameras, can also serve as crucial evidence to reveal manipulated regions within the authentic area. Thus, based on previous works, *the key to IML lies in capturing the artifacts by identifying non-semantic visible traces and low-level inconsistencies.*

However, convolution propagates information in a *collective* manner, making CNNs more suitable for semantic-

Methods	View	Training Dataset For Evaluation	Backbone	Resolution
ManTra-Net [30], 2019	BayarConv(Noise) SRM filter(Noise)	Private, 102,028 images	wider VGG	512×512
SPAN [13], 2020	BayarConv(Noise) SRM filter(Noise)	Private, 102,028 images (Copied parameters from ManTra-Net)	wider VGG self-attention	raw & 224×224 (resized feature)
CR-CNN [32], 2020	BayarConv(Noise) SRM filter(Noise)	Public: CASIA v2	mask R-CNN	short side to 600
GSR-Net [35], 2020	Edge Prediction	Public: CASIA v2	DeepLab	300×300
MVSS-Net [2], 2021	BayarConv(Noise) Sobel(Edge)	Public: CASIA v2 or Defacto	FCN	512×512
MM-Net [33], 2021	BayarConv(Noise)	Private: synthesized	mask R-CNN	short side to 800
TransForensics [10], 2021	-	Public: CASIA v2, COVERAGE and IMD2020	FCN + Transformer blocks	512×512
ObjectFormer [28], 2022	High-Frequency	Private: large synthesized	CNN + Transformer	256×256
<i>IML-ViT(This paper)</i>	Edge supervision	Public: CASIA v2	ViT	1024×1024 (zero-padding)

Table 1: **Overview of the state-of-the-art for image manipulation localization end-to-end models** *View* can be regarded as prior knowledge widely accepted in the field of manipulation detection. Edge information can better trace visible artifacts, while noise and high-frequency features mainly compare the low-level differences between tampered and authentic regions.

related tasks, such as object detection, rather than tracing non-semantic artifacts that often surround an object. Further, to identify low-level inconsistencies, we need to explicitly compare the relationships between different regions. But in deeper networks, CNNs may overlook global dependencies [22], rendering them less effective in capturing differences between regions. Given the weaknesses of CNN in non-semantic and long-distance modeling, we ask: *Is there any other optimal backbone for solving IML tasks?*

Considering the goal of capturing the feature discrepancies between the manipulated and authentic regions, we argue that self-attention should be a better solution regarding IML. *As self-attention can explicitly model relationships between any areas regardless of their visual semantic relevance, especially for non-adjacent regions.* The performance boost achieved by SPAN [13] highlights the effectiveness of integrating self-attention structures into convolutional layers. Furthermore, as artifacts are often distributed at the patch level rather than at the pixel or image level, Vision Transformer (ViT) [8] naturally becomes the ideal choice to trace artifacts and make comparisons.

While ViT may be suitable for IML tasks, directly applying the original ViT architecture is insufficient. We suggest that IML involves three key discrepancies from traditional segmentation tasks, which also have not yet received sufficient attention in previous IML methods, as supported by Table 1. These discrepancies are:

High resolution While semantic segmentation and IML share similar inputs and outputs, IML tasks are more information-intensive, focusing on detailed artifacts rather than macro-semantics at the object level. Existing methods use various extractors to trace artifacts, but their resizing methods already harm these first-hand artifacts. Therefore, preserving the *original resolution* of the images is crucial to

retain essential artifacts for the model to learn.

Edge supervision As mentioned earlier, IML’s primary focus lies in detecting the distinction between the tampered and authentic regions. This distinction is most pronounced at the boundary of the tampered region, whereas typical semantic segmentation tasks only require identifying information within the target region. From another perspective, it becomes evident that visible artifacts are more concentrated along the periphery of the tampered region rather than within it (as shown in Figure 1). Consequently, the IML task must guide the model to concentrate on the manipulated region’s edges and learn its distribution for better performance.

Multi-scale supervision The percentage of tampered area to the total area varies significantly across different IML datasets. CASIAv2 [7] contains a considerable amount of sky replacement tampering, whereas Defacto [23] mostly consists of small object manipulations. On average, CASIAv2 has 7.6% of pixels as tampered areas, while Defacto has only 1.7%. Additionally, IML datasets are labor-intensive and often limited in size, which poses challenges in bridging the gap between datasets. Therefore, incorporating multi-scale supervision from the pre-processing and model design stages is essential to enhance generalization across different datasets.

In this paper, we present IML-ViT, an end-to-end ViT-based model that solves IML tasks. Regarding the 3 key discrepancies, we devise IML-ViT with the following components: 1) a ViT which accepts high-resolution input. Most of the global attention block is replaced with windowed attention as the trade-off for time complexity. We initialized its parameters with ImageNet-1k MAE [11] pre-training; 2) a *simple feature pyramid* [18] network to introduce multi-scale supervision; 3) a morphology-based edge loss strat-

egy is proposed to ensure edge supervision. The overview of IML-ViT is shown in Figure 2.

To the best of our knowledge, ObjectFormer [28] and TransForensics [10] are the only Transformer-related models solving the IML tasks. However, their backbone distinguishes significantly from ViT, as will explain in the Related Works section. Thus, IML-ViT can be regarded as the pioneering model that utilizes ViT as the backbone for tackling IML tasks.

The experiments were conducted based on a common evaluation protocol [28, 36, 2, 30, 35] to measure the generalizability and performance of our IML-ViT. Model is trained on CASIAv2 [7] dataset and then test it on other 5 public datasets. The results demonstrate that IML-ViT has surpassed all SoTA models, indirectly validating the reliability of the three key aspects of IML proposed by us. Thus, we believe that IML-ViT is a powerful candidate to become a new SoTA model for IML.

With no specialized modules, IML-ViT has the potential to serve as a simple yet superior performance benchmark for IML and demonstrate that IML tasks can be solved without manually designed feature extractors or complicated feature fusion, promoting existing IML research into new research paradigms. In summary, our contributions are as follows:

- We reveal the essential discrepancies between IML and traditional segmentation tasks by raising the three uniqueness, which were overlooked by previous studies: high resolution, multi-scale, and edge supervision.
- Aiming at three uniqueness, we modify the components of ViT and establish the IML-ViT, the first ViT-based model for image manipulation localization.
- Extensive experiments show that IML-ViT outperforms state-of-the-art models in both F_1 and AUC scores on five public benchmark datasets. This verifies the solidity of the three uniqueness we proposed.

2. Related works

2.1. Transformer-based IML Method

Currently, there are two Transformer-based models in the field of IML, namely ObjectFormer [28] and TransForensics [10]. Though named “Trans” and “Former”, these two models are hardly in line with ViT in overall structures and design philosophies.

In particular, different from ViT directly embedding the patched images before encoding, both methods utilize several CNN layers to initially extract feature maps and subsequently employ Transformers for further encoding, leading to the neglect of crucial first-hand low-level information.

Moreover, in ObjectFormer(OF)’s encoder, the “query” inputs are learnable vectors representing object prototypes o_i , not image embeddings. As a result, it focuses on capturing dependencies between object prototypes and image tokens, whereas a standard ViT encoder solely models the dependencies between image embeddings. Besides, OF is pre-trained with a large tampering-oriented synthesized private dataset, while IML-ViT achieves superior performance with pre-training on the more accessible ImageNet-1k dataset and outperforms OF.

On the other hand, the primary distinction between TransForensics and ViT lies in how to apply Transformer blocks. While ViT uses these blocks sequentially, TransForensics employs them in parallel, wherein each feature map of an FCN output is decoded with a Transformer block, then fused together for the final output.

In short, IML-ViT can be considered the first IML method with a vanilla ViT as its backbone and could easily benefit from recently advanced algorithms related to ViT, proving that IML tasks do not require complex designs.

Paradigm of IML Research in the early years focused on single kind of manipulation detection, with studies on copy-move [3, 25], splicing [4, 14, 15], and Removal (Inpainting) [38], respectively. However, since the specific type of tampering is unknown in practice, after 2018, general manipulation detection has become the focus of research. Many existing works follow the paradigm of “feature extraction + backbone inference”, especially extractors to exploit tamper-related information from artifacts. Yang *et al.* design CR-CNN [32] with a noise-sensitive BayarConv [1] as the first convolution layer. Zhou *et al.* develop an SRM filter to mine the difference in noise distribution to support decision-making in their RGB-N networks[37]. And Wu *et al.* [30] and Hu *et al.* [13] combined SRM, BayarConv, and Conv2D as the first layer of their model. Besides noise-related extractors, Wang *et al.* [28] employ a DCT transform to extract high-frequency features, which are then combined with RGB features and fed into a transformer decoder. And Chen *et al.* suggest MVSS-Net [2] with a Sobel-supervised edge branch and a BayarConv noise branch. Dual attention is then utilized to fuse them.

Nevertheless, a feature may only be effective for a single type of tampering, e.g., noise is more sensitive to splicing from different images but less effective for copy-move from the same image. To avoid this issue, our IML-ViT is aiming to step out of the paradigm of “extraction + fusion” and let the model itself learn as much knowledge as possible from the datasets rather than simply rely on *priori knowledge*.

Resolution of IML Resolution is an important aspect but has always been neglected. Wu *et al.* [30] reported resize(re-scale) to images can do harm to the performance

of their model. However, we observed that most existing methods re-scale images to a uniform size during pre-processing for parallel training purposes (shown in *Resolution* column Table 1). In most cases, the images were down-sampled, destroying the aspect ratio and compressing the original information in the dataset. This manner can greatly affect the distribution of noise, edge, and high-frequency features in the raw image, then weaken the performance of the model. In this paper, we make a novel attempt of preserving the original resolution of the images as much as possible, by zero-padding them to 1024x1024 for parallel computation. This process can leave the freshest information for the model to mine the difference between the manipulated region and the authentic region, and make the best possible use of the dataset.

3. Proposed Method

In this section, we introduce our powerful IML-ViT paradigm, as shown in Figure 2, it consists of three main components: (1) a windowed ViT to balance the high-resolution inputs and the space complexity; (2) a *simple feature pyramid* network (SFPN) to introduce multi-scale features; and (3) a lightweight MLP decoder head with additional edge supervision, which aids in focusing on artifact-related features and ensures stable convergence.

3.1. ViT Backbone

High resolution The ViT Encoder aims to mine the detailed artifacts and explore the differences between the suspicious area. Thus, it is essential to **preserve the original resolution of each image** to avoid downsampling that could potentially distort the artifacts. However, when training in parallel, all images within a batch must have the same resolution. To reconcile these demands, we adopt a novel approach that has not been applied to any IML method before. Rather than simply rescaling images to the same size, we pad images and ground truth masks with zeros and place the image on the top-left side to match a larger constant resolution. This strategy maintains crucial low-level visual information of each image, allowing the model to explore better features instead of depending on handcrafted prior knowledge. To implement this approach, we first adjust the embedding dimensions of the ViT encoder to a larger scale.

Windowed attention To balance the computation cost from high resolution, we adopt a technique from previous works [17, 18], which periodically replaces part of the global attention blocks in ViT with windowed attention blocks. This method ensures global information propagation while reducing complexity.

MAE pre-train We initialize the ViT with parameters pre-trained on ImageNet-1k [5] with Masked Auto Encoder (MAE) [11]. This self-supervised method can greatly al-

leviate the over-fitting problem and helps the model generalize, supported by Table 3.

More specifically, we represent input images as $X \in \mathbb{R}^{3 \times h \times w}$, and ground truth masks as $M \in \mathbb{R}^{1 \times h \times w}$, where h and w correspond to the height and width of the image, respectively. We then pad them to $X_p \in \mathbb{R}^{3 \times H \times W}$ and $M_p \in \mathbb{R}^{1 \times H \times W}$. Balance with computational cost and the resolution of datasets we employ in Table 2, we take $H = W = 1024$ as constants in our implementation. Then X_p is passed into the windowed ViT-Base encoder with 12 layers, with a complete global attention block retained every 3 layers. The above process can be formulated as follows:

$$G_e = \mathcal{V}(X_p) \in \mathbb{R}^{768 \times \frac{H}{16} \times \frac{W}{16}} \quad (1)$$

where \mathcal{V} denotes the ViT, and G_e stands for encoded feature map. The number of channels, 768, is to keep the information density the same as the RGB image at the input, as $768 \times \frac{H}{16} \times \frac{W}{16} = 3 \times H \times W$.

3.2. Simple Feature Pyramid

To introduce multi-scale supervision, we adopt the *simple feature pyramid* network (SFPN) after the ViT encoder, which was suggested in ViTDet [34]. This method takes the single output feature map G_e from ViT, and then uses a series of convolutional and deconvolutional layers to perform up-sampling and down-sampling to obtain multi-scale feature maps:

$$F_i = \mathcal{C}_i(G_e) \in \mathbb{R}^{C_s \times \frac{H}{2^{i+2}} \times \frac{W}{2^{i+2}}}, i \in \{1, 2, 3, 4\} \quad (2)$$

where \mathcal{C}_i denotes the convolution series, and C_s is the output channel dimension for each layer in SFPN. This multi-scale method does not change the base structure of ViT, which allowed us easily introduce recently advanced algorithms to the backbone.

3.3. Light-weight Predict Head

For the final prediction, we aimed to design a model that is simple enough to reduce memory consumption while also demonstrating that the improvements come from the advanced design in the ViT Encoder and the multi-scale supervision. Based on these ideas, we adopted the decoder design from SegFormer [31], which outputs a smaller predicted mask M_e with a resolution of $1 \times \frac{H}{4} \times \frac{W}{4}$. The lightweight All-MLP decoder first applies a linear layer to unify the channel dimension. It then up-samples all the features to the same resolution of $C_D \times \frac{H}{4} \times \frac{W}{4}$ with bilinear interpolation, and concatenates all the features together, as shown in Figure 3. Finally, a series of linear layers is applied to fuse all the layers and make the final prediction. We can formulate the prediction head as follows:

$$P = MLP\{\odot_i(W_i F_i + b_i)\} \in \mathbb{R}^{\frac{H}{4} \times \frac{W}{4} \times 1} \quad (3)$$

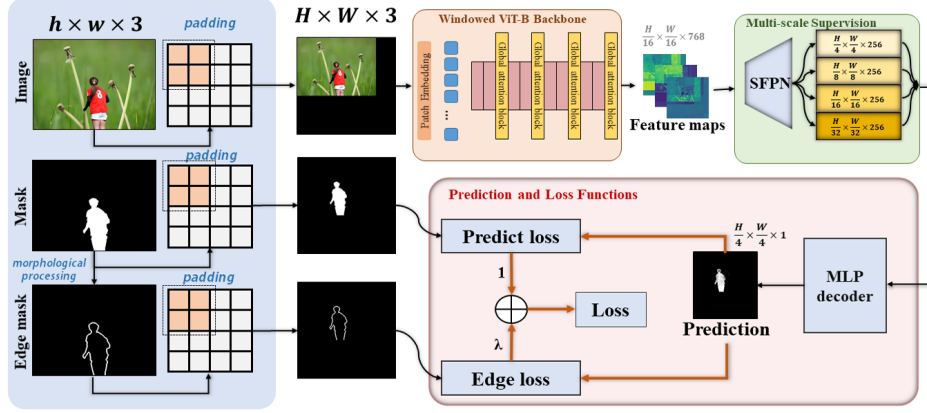


Figure 2: Overview of the general structure of IML-ViT.

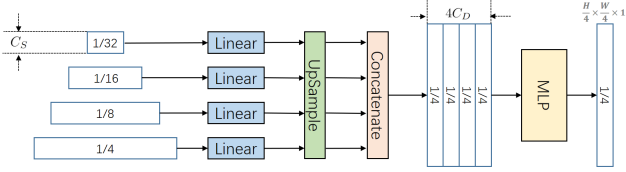


Figure 3: Diagrams of the predict head. The rectangles on the left represent the output of SFPN.

Here, P represents the predicted probability map for the manipulated area; \odot denotes concatenation operation, and MLP refers to an MLP module.

3.4. Edge Supervision Loss

To account for the fact that artifacts are typically more prevalent at the edges of tampered regions, where the differences between manipulated and authentic areas are most noticeable, we developed a strategy that places greater emphasis on the boundary region of the manipulated area. Specifically, we generate a binary edge mask M^* from the original mask image M using mathematical morphology operations including dilation (\oplus) and erosion (\ominus) [26], followed by taking the absolute values of the result. The formula we use to generate the edge mask is:

$$M^* = |(M \ominus B(k)) - (M \oplus B(k))| \quad (4)$$

where, $B(x)$ generates a $(2x + 1) \times (2x + 1)$ cross matrix, where only the x^{th} column and x^{th} row have a value of 1, while the rest of the matrix contains 0s. The integer value x is selected to be approximately equal to the width of the white area in the boundary mask. Examples of the edge mask generated using this approach are shown in Figure 4.

Combined Loss To compute the loss function, we first pad the ground-truth mask M and the edge mask M^* to the size of $H \times W$, and refer to them as M_p and M_p^* , respectively.

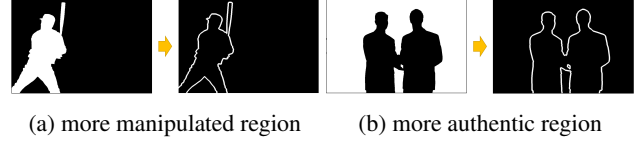


Figure 4: Examples of generating the edge mask M^* , white represent for manipulated area, k is set to 5 while the image size is 1024×682 . The absolute value operation ensures that whether the tampered region dominates or the non-tampered region dominates, the mask only emphasizes the junction of the two.

We then calculate the final loss using the following formula:

$$\mathcal{L} = \mathcal{L}_{seg}(P, M_p) + \lambda \cdot \mathcal{L}_{edge}(P * M_p^*, M_p * M_p^*) \quad (5)$$

where $*$ denotes the point-wise product, which masks the original image. Both \mathcal{L}_{seg} and \mathcal{L}_{edge} are binary cross-entropy loss functions, and λ is a hyper-parameter that controls the balance between the segmentation and edge detection losses. By default, we set $\lambda = 20$ to guide the model to focus on the edge regions.

While this strategy is straightforward, as will discuss in the Experiments section, it remarkably accelerates model convergence, stabilizes the training process, and mitigates potential NaN (Not-a-Number) issues. Therefore, we consider this strategy to be a powerful prior knowledge for IML problems, deserving attention in future research.

4. Experiments

4.1. Experimental setup

Datasets To make a fair comparison with state-of-the-art, we mainly evaluate the performance of our model based on a commonly used protocol [2, 35, 13] for image tampering localization. We train the model on the CASIAv2 [7]

dataset¹ and then test it on other smaller public datasets including CASIAv1 [7], NIST16 [9], COVERAGE [29], Columbia [12] and Defacto [23], see Table 2. However, there are no authentic images as negative examples in the Defacto dataset. Following the approach of MVSS-Net, we randomly selected 6000 untouched images from MS-COCO dataset [19] and combined them with 6000 images from Defacto to create the Defacto-12k dataset for validation.

Usage	Dataset	Type		Manipulation type			Resolution	
		Authentic	Manipulated	copymv	spl	inpa	min	max
Train	CASIAv	7491	5063	3235	1828	0	240	800
Test	CASIAv1	800	920	459	461	0	256	384
	NIST16	0	564	68	288	208	480	5616
	COVERAGE	100	100	100	0	0	158	572
	Defacto-12k	6000	6000	2000	2000	2000	120	640
	Columbia	183	180	0	180	0	568	1152

Table 2: Details of six datasets in our experiments

Evaluation Criteria We evaluate our model using pixel-level F_1 score with a fixed threshold 0.5 and Area Under the Curve (AUC), which are commonly used evaluation metrics in previous works. However, it’s worth noting that AUC can be influenced by an excessive number of true negative pixels in common IML datasets, leading to an overestimation of model performance. Nevertheless, our model achieves state-of-the-art performance in both F_1 score and AUC.

In some previous methods, *optimal F1 score* is used for evaluation, where the best F_1 score is selected by testing the prediction probability map at different thresholds. However, this approach becomes impractical in real-world scenarios since the optimal threshold for the real-world distribution is typically unknown. Instead, we report the pixel-level F_1 score using a uniform threshold of 0.5, providing a more practical metric for evaluating the model’s performance.

Implementation Our IML-ViT model is implemented with PyTorch and trained on NVIDIA RTX 3090 GPUs for 200 epochs with a batch size of 1 in each GPU (16GB of graphics memory). Accumulate batch strategy is applied with a size of 32. We pad all images to a resolution of 1024x1024, except for those that exceed this limit. For the larger images, we resized them to the longer side to 1024 and maintain their aspect ratio. Before training, following MVSS-Net, common data augmentation techniques were applied, including re-scaling, flipping, blurring, rotation, and various naive manipulations (e.g., randomly copy-moving or inpainting rectangular areas within a single image). We initialize ViT-B with MAE pre-trained weights on ImageNet-1k and used the AdamW optimizer [21] with a base learning

¹We noticed some resolution errors in the public CASIAv2 dataset. Therefore, we have released an adjusted version of CASIAv2 with corrected ground truth. Details can be found at <https://github.com/SunnyHaze/CASIA2.0-Corrected-Groundtruth>

rate of 1e-4. We scheduled the learning rate using a cosine decay strategy [20]. The early stop technique was employed during training.

4.2. Ablation Studies

To better evaluate the contributions of each component to the model performance, we conducted experiments with multiple settings and compare them with a *full setup* to test the four aspects we are most concerned about. For *initialization*, besides *full setup* with MAE pre-training on ImageNet-1k, we test Xavier initialization and ordinary ViT pre-training on ImageNet-21k by classification. To explore the impact of *high resolution*, we simply resized all images to 512x512 during training instead of our padding strategy. For *edge supervision*, and *multi-scale supervision*, we evaluate them by removing the respective structures from the model.

During ablation studies, We trained model *only* with manipulated images in CASIAv2 and evaluate its pixel-level F_1 score on CASIAv1, COVERAGE, Columbia, and NIST16 datasets. The experiment setups and the results are shown in Table 3. In conclusion, our findings are:

MAE pretrain is mandatory. Indeed, dataset insufficiency is a significant challenge in building ViT-based IML methods. As shown in Table 2, public data sets for IML are small in size, which cannot satisfy the appetite of vanilla ViT. As shown in *w/o MAE* aspects in Table 3, the use of Xavier initialization to train the model resulted in complete non-convergence. However, while regular ViT pre-training initialization with Imagenet-21k achieves acceptable performance on CASIAv1 which is homologous to CASIAv2, exhibits poor generalization ability on other non-homology datasets. The results indicate that MAE greatly alleviated the problem of non-convergence and over-fitting of ViT on small datasets. This suggests that MAE pre-training is indispensable for ViT-based image manipulation localization, and demonstrates that MAE is a powerful and effective method for downstream tasks with limited datasets.

Edge supervision is crucial. The performance of IML-ViT without edge loss shows significant variability with different random seeds, all leading to gradient collapse eventually, where the F_1 score reaches 0, and the loss becomes NaN, as shown in Figure 5. On the other hand, when employing edge loss, all performance plots for IML-ViT exhibit consistent behavior similar to the blue line in Figure 5, enabling fast convergence and smooth training up to 200 epochs. Furthermore, Table 3 confirms the effectiveness of edge loss in contributing to the final performance. In summary, these results demonstrate that edge supervision effectively stabilizes IML-ViT convergence and can serve as highly efficient prior knowledge for IML problems.

Test Goal	init method	Components			CASIAv1		Coverage		Columbia		NIST16		MAEN	
		H-Reso	S-FPN	Edge	F1	AUC	F1	AUC	F1	AUC	F1	AUC	F1	AUC
w/o MAE	Xavier	+	+	+	0.1035	-	0.0439	-	0.0744	-	0.0632	-	0.0713	-
	ViT-B ImNet-21k	+	+	+	0.5114	-	0.1854	-	0.2287	-	0.1811	-	0.2767	-
w/o high resolution	MAE ImNet-1k	-	+	+	0.5061	0.8166	0.2324	0.825	0.5409	0.842	0.2987	0.8212	0.3945	0.8262
w/o multi-scale	MAE ImNet-1k	+	-	+	0.5996	0.8627	0.4457	0.8352	0.6125	0.8350	0.1841	0.6767	0.4605	0.8024
w/o edge supervision	MAE ImNet-1k	+	+	-	0.5432	0.8573	0.2688	0.8272	0.3008	0.7617	0.2347	0.7078	0.3369	0.7885
Full setup	MAE ImNet-1k	+	+	+	0.5886	0.8668	0.3277	0.8264	0.7445	0.9076	0.2993	0.7706	0.4900	0.8429

Table 3: **Ablation study of IML-ViT.** Each model is trained for 200 epochs on CASIAv2 dataset **without authentic images.** Best scores are marked in bold.

Method	Pixel-level F_1 score					
	CASIAv1	Columbia	NIST16	Coverage	Defacto-12k	MEAN
HP-FCN*, ICCV19 [16]	0.154	0.067	0.121	0.003	0.055	0.080
ManTra-Net*, CVPR19 [30]	0.155	0.364	0	0.286	0.155	0.192
CR-CNN*, ICME20 [32]	0.405	0.436	0.238	0.291	0.132	0.300
GSR-Net*, AAI20 [35]	0.387	0.613	0.283	0.285	0.051	0.324
MVSS-Net*, ICCV21 [2]	0.452	0.638	0.292	0.453	0.137	0.394
MVSS-Net (re-trained)	0.435	0.303	0.203	0.329	0.097	0.270
MVSS-Net++*, PAMI22 [6]	0.513	0.660	0.304	0.482	0.095	0.411
IML-ViT (ours)	0.658	0.836	0.339	0.425	0.156	0.482

Table 4: **Cross-datasets evaluation of SoTA models.** Except for ManTra-Net and HP-FCN, which trained on a privately synthesized dataset, all the methods were trained on CASIAv2 datasets. The best scores are highlighted in bold. Symbol '*' marks the results are quoted from MVSS-Net paper [2]. We re-train MVSS-Net with their official-released code.

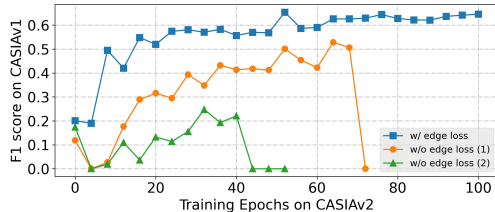


Figure 5: **Impact of the proposed edge loss on training.** Note that settings here follow Table 4 instead of Table 3.

High resolution is effective for artifacts. The improved performance shown in Table 3 for the *full setup* model across four datasets validates the effectiveness of the high-resolution strategy. However, it is essential to note that the NIST16 dataset shows limited improvement when using higher resolutions. This observation can be attributed to the fact that the NIST16 dataset contains numerous images with resolutions exceeding 2000, and down-sampling these images to 1024 for testing may lead to considerable distortion of the original artifacts, consequently reducing the effectiveness of learned features. Nevertheless, when considering the SoTA score achieved, it becomes evident that IML-ViT can flexibly infer the manipulated area based on the richness of different information types.

Multi-scale supervision helps generalize. However, af-

ter applying the SFPN, there is not much improvement in average F_1 , even the performance slightly decreases on CASIAv1 and Coverage. But in exchange, the results on NIST16 gain a larger boost. Since CASIAv2 and CASIAv1 are homologous datasets, a good performance on CASIAv1 cannot reflect the generalization ability well. Coverage, as a dataset with only 100 splicing images, is somewhat limited as well. Therefore, it is a worthwhile trade-off to achieve more improvement on NIST16, which has more images and diverse manipulation types. This validates that SFPN does bring certain generalization performances to the model.

4.3. Comparison with SoTA

Evaluation barrier While recent studies have introduced numerous state-of-the-art models, it remains challenging to compare them on an equal footing. This is partly due to the lack of publicly available code for the models and training processes [13, 28], as well as the utilization of massive synthesized datasets that are inaccessible to the wider research community [30, 33]. Therefore, we urge for the adoption of open-source to the community and call for the generation strategies for large-scale datasets can be assessed separately from the model performance itself. Such measures are vital for ensuring fairness and promoting continued advancements in this field. To demonstrate the potential of IML-ViT as an effective benchmark, we conduct a comprehensive comparison with existing models in a fair manner.

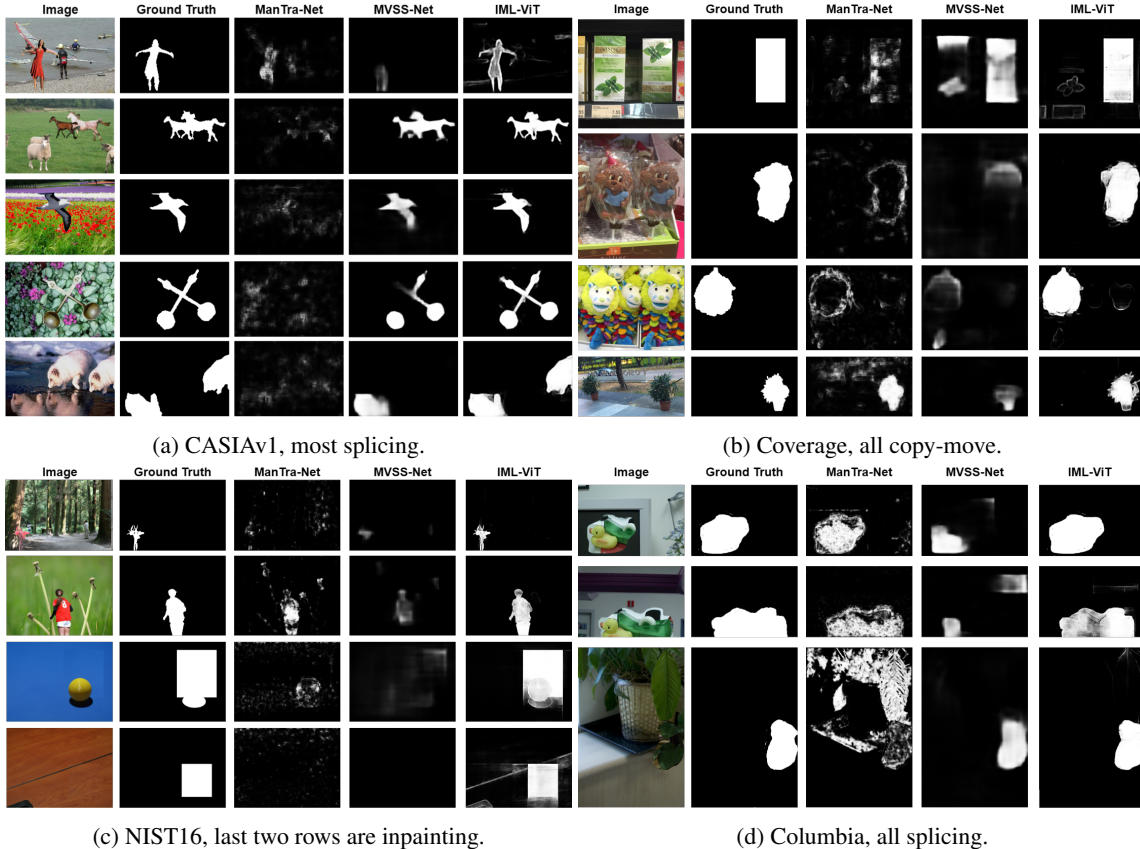


Figure 6: **Testing results trained with CASIAv2 on 4 datasets of IML-ViT compare to ManTra-Net and MVSS-Net.** Each dataset has its preference for manipulation types. Columns from left to right are: input image, ground-truth, Mantra-Net, MVSS-Net and IML-ViT (ours). Zoom in for a better view.

Method	Pre-train	$F_1(\%)$
RGB-N, CVPR18 [36]	ImageNet	40.8
SPAN, ECCV20 [13]	Private synthesized dataset	38.2
Objectformer, CVPR22 [28]	Private synthesized dataset	57.9
<i>IML-ViT(Ours)</i>	MAE on ImageNet-1k	73.4

Table 5: **Performance comparison with Closed-source methods** All the methods above are fine-tuning with CASIAv2 and are tested with the CASIAv1 dataset.

Method	CASIAv1	Coverage	Columbia	NIST16	MEAN
ObjectFormer	0.882	-	-	-	-
CFL-Net	0.863	-	-	0.799	-
<i>IML-ViT(Ours)</i>	0.931	0.918	0.962	0.818	0.917

Table 6: **Comparison of AUC trained on CASIAv2.**

Cross-dataset comparison Since MVSS-Net [2] has already conducted a detailed evaluation on a fair cross-dataset protocol, we directly quote their results here and train our models with the same protocol, i.e. training on both authen-

tic and manipulated images of CASIAv2 dataset and testing on public datasets. The results measured by F_1 score are listed respectively in Table 4. We also list comparison with some closed-source method that only reports their F1 score tested on CASIAv1 in Table 5.

Moreover, ObjectFormer [28] and CFL-Net [24] evaluate their models fine-tuning with CASIAv2 on AUC. Although this metric may overestimate the models, IML-ViT has still surpassed them, as shown in Table 6.

Overall, our model has achieved state-of-the-art performance compared to existing models evaluated under this fair cross-dataset protocol. Figure 6 qualitatively illustrates the high-quality and clear boundary of our model trained on CASIAv2 and tested on various datasets under different preferences of manipulation types.

Mix-dataset comparison Some methods reported their performance based on mixed datasets, which were randomly split into train-validate-test sets, introducing sampling bias. Particularly, in the case of NIST16, there exists a consid-

Method	Datasets (Train/validate/test split)	Pixel-level AUC				Pixel-level F_1	
		COVER	NIST16	CASIA	IMD-20	CASIA	COVER
TransForesinc, ICCV21	COVER + CASIA + IMD20 (8:1:1)	0.884	-	0.850	0.848	0.627	0.674
<i>IML-ViT(Ours)</i>	COVER + CASIA + IMD20 (8:1:1)	0.912	0.821*	0.961	0.943	0.825	0.815
ObjectFormer, CVPR22	COVER(4:1); NIST(4:1); CASIA(v2:v1)	0.957	0.996	0.882	-	0.579	0.758
CF-Net, WACV23	NIST16 + CASIA + IMD20 (8:1:1)	-	0.997	0.863	0.899	-	-
<i>IML-ViT(Ours)</i>	NIST16 + CASIA + IMD20 (8:1:1)	0.801*	0.997	0.959	0.941	0.820	0.505*

Table 7: **Mix-dataset results.** * marks cross-dataset results.

erable number of duplicated samples, and random splitting might cause the same image to appear repeatedly in both the train and test sets, resulting in artificially inflated metrics. This makes them unsuitable as reliable benchmarks. Anyway, results in Table 7 show that, under the same evaluation criteria, IML-ViT also outperforms them.

4.4. Robustness Evaluation

JPEG compression and Gaussian Blur are the common attack method for Image manipulation localization. Hence we further carried out experiments on the resistance of these two operations on CASIAv1. The evaluation results² are shown in Figure 7. The IML-ViT exhibited excellent resistance to JPEG compression and Gaussian blur and consistently maintained the best performance of the five models.

achieves SoTA performance and generalization ability, validating the reliability of the three core elements of the IML task proposed in this study: high resolution, multi-scale, and edge supervision. Further, IML-ViT proves the effectiveness of self-attention in capturing non-semantic artifacts. Its simple structure also makes it a promising benchmark in this field.

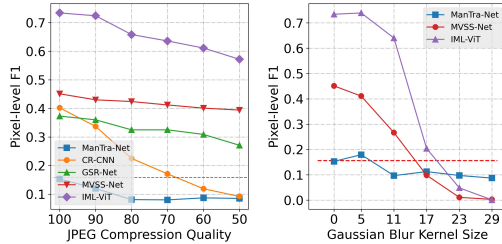


Figure 7: **Robustness Evaluation against JPEG compression and Gaussian blur on CASIAv1.** The red dashed line represents the F_1 score when all predictions are classified as positive. When the result is lower than this line, we consider the model to be less effective than random guessing and losing its localization ability. Our model has a later entry of the F_1 score into the baseline value compared to other models, and it consistently maintains a relatively high position, proving its better resistance.

5. Conclusions

This paper introduces IML-ViT, the first image manipulation localization model based on ViT. Extensive experiments on five public datasets demonstrate that IML-ViT

²Performance against JPEG compression is quoted from MVSS-Net, while performance against Gaussian Blur is retested by us using the publicly available model because we found a significant discrepancy between our tests and the performance reported in their paper.

References

- [1] Belhassen Bayar and Matthew C. Stamm. Constrained convolutional neural networks: A new approach towards general purpose image manipulation detection. *IEEE Transactions on Information Forensics and Security*, 13(11):2691–2706, Nov 2018. **3**
- [2] Xinru Chen, Chengbo Dong, Jiaqi Ji, Juan Cao, and Xirong Li. Image manipulation detection by multi-view multi-scale supervision. In *2021 IEEE/CVF International Conference on Computer Vision (ICCV)*, page 14165–14173, Montreal, QC, Canada, Oct 2021. IEEE. **2, 3, 5, 7, 8**
- [3] Davide Cozzolino, Giovanni Poggi, and Luisa Verdoliva. Efficient dense-field copy–move forgery detection. *IEEE Transactions on Information Forensics and Security*, 10(11):2284–2297, Nov 2015. **3**
- [4] Davide Cozzolino, Giovanni Poggi, and Luisa Verdoliva. Splicebuster: A new blind image splicing detector. In *2015 IEEE International Workshop on Information Forensics and Security (WIFS)*, page 1–6, Roma, Italy, Nov 2015. IEEE. **3**
- [5] Jia Deng, Wei Dong, Richard Socher, Li-Jia Li, Kai Li, and Li Fei-Fei. Imagenet: A large-scale hierarchical image database. In *2009 IEEE Conference on Computer Vision and Pattern Recognition*, page 248–255, Miami, FL, Jun 2009. IEEE. **4**
- [6] Chengbo Dong, Xinru Chen, Ruohan Hu, Juan Cao, and Xirong Li. Mvss-net: Multi-view multi-scale supervised networks for image manipulation detection. *IEEE Transactions on Pattern Analysis and Machine Intelligence*, page 1–14, 2022. **7**
- [7] Jing Dong, Wei Wang, and Tieniu Tan. Casia image tampering detection evaluation database. In *2013 IEEE China Summit and International Conference on Signal and Information Processing*, page 422–426, Beijing, China, Jul 2013. IEEE. **2, 3, 5, 6**
- [8] Alexey Dosovitskiy, Lucas Beyer, Alexander Kolesnikov, Dirk Weissenborn, Xiaohua Zhai, Thomas Unterthiner, Mostafa Dehghani, Matthias Minderer, Georg Heigold, Sylvain Gelly, Jakob Uszkoreit, and Neil Houlsby. An image is worth 16x16 words: Transformers for image recognition at scale. (arXiv:2010.11929), Jun 2021. arXiv:2010.11929 [cs]. **2**
- [9] Haiying Guan, Mark Kozak, Eric Robertson, Yooyoung Lee, Amy N. Yates, Andrew Delgado, Daniel Zhou, Timothee Kheyrkhah, Jeff Smith, and Jonathan Fiscus. Mfc datasets: Large-scale benchmark datasets for media forensic challenge evaluation. In *2019 IEEE Winter Applications of Computer Vision Workshops (WACVW)*, page 63–72, Waikoloa Village, HI, USA, Jan 2019. IEEE. **6**
- [10] Jing Hao, Zhixin Zhang, Shicai Yang, Di Xie, and Shiliang Pu. Transforensics: Image forgery localization with dense self-attention. In *2021 IEEE/CVF International Conference on Computer Vision (ICCV)*, page 15035–15044, Montreal, QC, Canada, Oct 2021. IEEE. **2, 3**
- [11] Kaiming He, Xinlei Chen, Saining Xie, Yanghao Li, Piotr Dollar, and Ross Girshick. Masked autoencoders are scalable vision learners. In *2022 IEEE/CVF Conference on Computer Vision and Pattern Recognition (CVPR)*, page 15979–15988, New Orleans, LA, USA, Jun 2022. IEEE. **2, 4**
- [12] Yu-feng Hsu and Shih-fu Chang. Detecting image splicing using geometry invariants and camera characteristics consistency. In *2006 IEEE International Conference on Multimedia and Expo*, page 549–552, Toronto, ON, Canada, Jul 2006. IEEE. **6**
- [13] Xuefeng Hu, Zhihan Zhang, Zhenye Jiang, Syomantak Chaudhuri, Zhenheng Yang, and Ram Nevatia. Span: Spatial pyramid attention network for image manipulation localization. In *Computer Vision—ECCV 2020: 16th European Conference, Glasgow, UK, August 23–28, 2020, Proceedings, Part XXI 16*, pages 312–328. Springer, 2020. **2, 3, 5, 7, 8**
- [14] Minyoung Huh, Andrew Liu, Andrew Owens, and Alexei A. Efros. *Fighting Fake News: Image Splice Detection via Learned Self-Consistency*, volume 11215 of *Lecture Notes in Computer Science*, page 106–124. Springer International Publishing, Cham, 2018. **3**
- [15] Vladimir V Kniaz, Vladimir Knyaz, and Fabio Remondino. The point where reality meets fantasy: Mixed adversarial generators for image splice detection. **3**
- [16] Haodong Li and Jiwu Huang. Localization of deep inpainting using high-pass fully convolutional network. In *2019 IEEE/CVF International Conference on Computer Vision (ICCV)*, page 8300–8309, Seoul, Korea (South), Oct 2019. IEEE. **7**
- [17] Yanghao Li, Chao-Yuan Wu, Haoqi Fan, Karttikeya Mangalam, Bo Xiong, Jitendra Malik, and Christoph Feichtenhofer. Mvitv2: Improved multiscale vision transformers for classification and detection. In *2022 IEEE/CVF Conference on Computer Vision and Pattern Recognition (CVPR)*, page 4794–4804, New Orleans, LA, USA, Jun 2022. IEEE. **4**
- [18] Yanghao Li, Saining Xie, Xinlei Chen, Piotr Dollar, Kaiming He, and Ross Girshick. Benchmarking detection transfer learning with vision transformers. (arXiv:2111.11429), Nov 2021. arXiv:2111.11429 [cs]. **2, 4**
- [19] Tsung-Yi Lin, Michael Maire, Serge Belongie, James Hays, Pietro Perona, Deva Ramanan, Piotr Dollár, and C. Lawrence Zitnick. *Microsoft COCO: Common Objects in Context*, volume 8693 of *Lecture Notes in Computer Science*, page 740–755. Springer International Publishing, Cham, 2014. **6**
- [20] Ilya Loshchilov and Frank Hutter. Sgdr: Stochastic gradient descent with warm restarts. (arXiv:1608.03983), May 2017. arXiv:1608.03983 [cs, math]. **6**
- [21] Ilya Loshchilov and Frank Hutter. Decoupled weight decay regularization. (arXiv:1711.05101), Jan 2019. arXiv:1711.05101 [cs, math]. **6**
- [22] Wenjie Luo, Yujia Li, Raquel Urtasun, and Richard Zemel. Understanding the effective receptive field in deep convolutional neural networks. In D. Lee, M. Sugiyama, U. Luxburg, I. Guyon, and R. Garnett, editors, *Advances in Neural Information Processing Systems*, volume 29. Curran Associates, Inc., 2016. **2**
- [23] Gael Mahfoudi, Badr Tajini, Florent Retraint, Frederic Morain-Nicolier, Jean Luc Dugelay, and Marc Pic. Defacto: Image and face manipulation dataset. In *2019 27th Euro-*

- pean Signal Processing Conference (EUSIPCO), page 1–5, A Coruna, Spain, Sep 2019. IEEE. 2, 6
- [24] Fahim Faisal Niloy, Kishor Kumar Bhaumik, and Simon S. Woo. Cfl-net: Image forgery localization using contrastive learning. In *2023 IEEE/CVF Winter Conference on Applications of Computer Vision (WACV)*, page 4631–4640, Waikoloa, HI, USA, Jan 2023. IEEE. 8
- [25] Yuan Rao and Jiangqun Ni. A deep learning approach to detection of splicing and copy-move forgeries in images. In *2016 IEEE International Workshop on Information Forensics and Security (WIFS)*, page 1–6, Abu Dhabi, United Arab Emirates, Dec 2016. IEEE. 3
- [26] Jean Serra. Image analysis and mathematical morphology, 1983. 5
- [27] Luisa Verdoliva. Media forensics and deepfakes: An overview. *IEEE Journal of Selected Topics in Signal Processing*, 14(5):910–932, Aug 2020. 1
- [28] Junke Wang, Zuxuan Wu, Jingjing Chen, Xintong Han, Abhinav Shrivastava, Ser-Nam Lim, and Yu-Gang Jiang. Objectformer for image manipulation detection and localization. In *2022 IEEE/CVF Conference on Computer Vision and Pattern Recognition (CVPR)*, page 2354–2363, New Orleans, LA, USA, Jun 2022. IEEE. 2, 3, 7, 8
- [29] Bihan Wen, Ye Zhu, Ramanathan Subramanian, Tian-Tsong Ng, Xuanjing Shen, and Stefan Winkler. Coverage — a novel database for copy-move forgery detection. In *2016 IEEE International Conference on Image Processing (ICIP)*, page 161–165, Phoenix, AZ, USA, Sep 2016. IEEE. 6
- [30] Yue Wu, Wael AbdAlmageed, and Premkumar Natarajan. Mantra-net: Manipulation tracing network for detection and localization of image forgeries with anomalous features. In *2019 IEEE/CVF Conference on Computer Vision and Pattern Recognition (CVPR)*, page 9535–9544, Long Beach, CA, USA, Jun 2019. IEEE. 1, 2, 3, 7
- [31] Enze Xie, Wenhai Wang, Zhiding Yu, Anima Anandkumar, Jose M. Alvarez, and Ping Luo. Segformer: Simple and efficient design for semantic segmentation with transformers. (arXiv:2105.15203), Oct 2021. arXiv:2105.15203 [cs]. 4
- [32] Chao Yang, Huizhou Li, Fangting Lin, Bin Jiang, and Hao Zhao. Constrained r-cnn: A general image manipulation detection model. In *2020 IEEE International conference on multimedia and expo (ICME)*, page 1–6. IEEE, 2020. 2, 3, 7
- [33] Chao Yang, Zhiyu Wang, Huawei Shen, Huizhou Li, and Bin Jiang. Multi-modality image manipulation detection. In *2021 IEEE International Conference on Multimedia and Expo (ICME)*, page 1–6, Shenzhen, China, Jul 2021. IEEE. 2, 7
- [34] Li Yanghao, Hanzi Mao, Ross Girshick, and Kaiming He. Exploring plain vision transformer backbones for object detection. (arXiv:2203.16527), Jun 2022. arXiv:2203.16527 [cs]. 4
- [35] Peng Zhou, Bor-Chun Chen, Xintong Han, Mahyar Najibi, Abhinav Shrivastava, Ser-Nam Lim, and Larry Davis. Generate, segment, and refine: Towards generic manipulation segmentation. *Proceedings of the AAAI Conference on Artificial Intelligence*, 34(07):13058–13065, Apr 2020. 2, 3, 5, 7
- [36] Peng Zhou, Xintong Han, Vlad I. Morariu, and Larry S. Davis. Learning rich features for image manipulation detection. In *2018 IEEE/CVF Conference on Computer Vision and Pattern Recognition*, page 1053–1061, Salt Lake City, UT, USA, Jun 2018. IEEE. 3, 8
- [37] Peng Zhou, Xintong Han, Vlad I. Morariu, and Larry S. Davis. Learning rich features for image manipulation detection. In *2018 IEEE/CVF Conference on Computer Vision and Pattern Recognition*, page 1053–1061, Salt Lake City, UT, USA, Jun 2018. IEEE. 3
- [38] Xinshan Zhu, Yongjun Qian, Xianfeng Zhao, Biao Sun, and Ya Sun. A deep learning approach to patch-based image inpainting forensics. *Signal Processing: Image Communication*, 67:90–99, Sep 2018. 3

A. Implementation Details

High-resolution ViT-Base Mostly following the original Vision Transformer, we implemented our model with a stack of Transformer blocks stacking together. Each block has a self-attention head and an MLP block in it, both having LayerNorm(LN). Every two windowed attention blocks are followed by a global attention block. The windowed attention block only computes self-attention in a small window, while the global attention block ensures global information propagation. Although we introduce the windowed attention, it only affects the self-attention manner but doesn't change the linear projection for Q, K, and V. Therefore, we can directly apply the MAE pre-trained parameters from a vanilla ViT with all global attention to this Windowed attention model without any extra process. Detailed structures are shown in Table 8.

Configs	Value
patch size	16
embedding dim	768
depth	12
number of heads	12
input size	3x1024x1024
window size	14
Norm layer	LN
Global block indexes	2,5,8,11
Output shape	768x64x64

Table 8: Detailed structure of windowed ViT-Base

Simple Feature Pyramid After getting the output from ViT-B, SFPN using a series of convolution, pooling, or deconvolution(ConvTranspose2D) layers to sample it to feature maps with 256 channels and in a scale of {4.0, 2.0, 1.0, 0.5, 0.25} compared to the resolution of input feature maps(768x64x64). Each layer is followed by LayerNorm. Detailed structures can see in Table 9.

Scales	Layers & channels of feature maps
4.0	768 ConvT 384 ConvT 192 Conv(1,1) 256 Conv(3,3) 256
2.0	768 ConvT 384 Conv(1,1) 256 Conv(3,3) 256
1.0	768 Conv(1,1) 256 Conv(3,3) 256
0.5	768 maxpool2D 384 Conv(1,1) 256 Conv(3,3) 256
0.25	768 maxpool2D 384 Conv(1,1) 256 Conv(3,3) 256 maxpool2D 256

Table 9: Detailed structure of Simple feature pyramid *ConvT* denotes for ConvTranspose2D with kernel size of 2 and stride of 2; Conv(x,x) indicate that a Conv2D layer with kernel size of x; and maxpool2D has also a kernel size of 2. The number shown between layers indicates the number of channels for its respective feature map between layers

Prediction head We test for the performance of different norm layer used in prediction head, result are shown in Table 10.

Training settings Since our model could only train with a single image for a batch, we apply to accumulate gradient

Norm type	F1 score				
	CASIAv1	Columbia	Coverage	NIST16	Average
No Norm	0.6081	0.6026	0.4361	0.1936	0.4601
Layer Norm	0.6013	0.5487	0.4066	0.254	0.45265
Batch Norm	0.5939	0.6607	0.4128	0.2649	0.483075

Table 10: Testing for Norm in Predict Head Implementation is followed to ablation study in the main paper.

during training, i.e. update the parameters every 32 images during training. Besides, we adopt the early stop method during training. Evaluate the performance on the F1 score for CASIAv1, and stop training when there is no improvement for 15 epochs. Other configs are described in Table 11.

Configs	Value
batch size	1
accumulate batch size	32
epochs	200
warm up epochs	4
optimizer	AdamW
optimizer momentum	$\beta_1, \beta_2 = 0.9, 0.95$
base learning rate	1e-4
minimum learning rate	5e-7
learning rate schedule	cosine decay
weight decay	0.05

Table 11: Training settings for IML-ViT

B. Visualization of Feature maps

To gain a deeper understanding of our IML-ViT model's inner workings, we present visualizations of feature maps between layers by calculating the average channel dimensions of the feature map. The outcomes are displayed in Figure 8. This visualization process allows us to shed light on the model's functioning and provides valuable insights into its mechanisms.

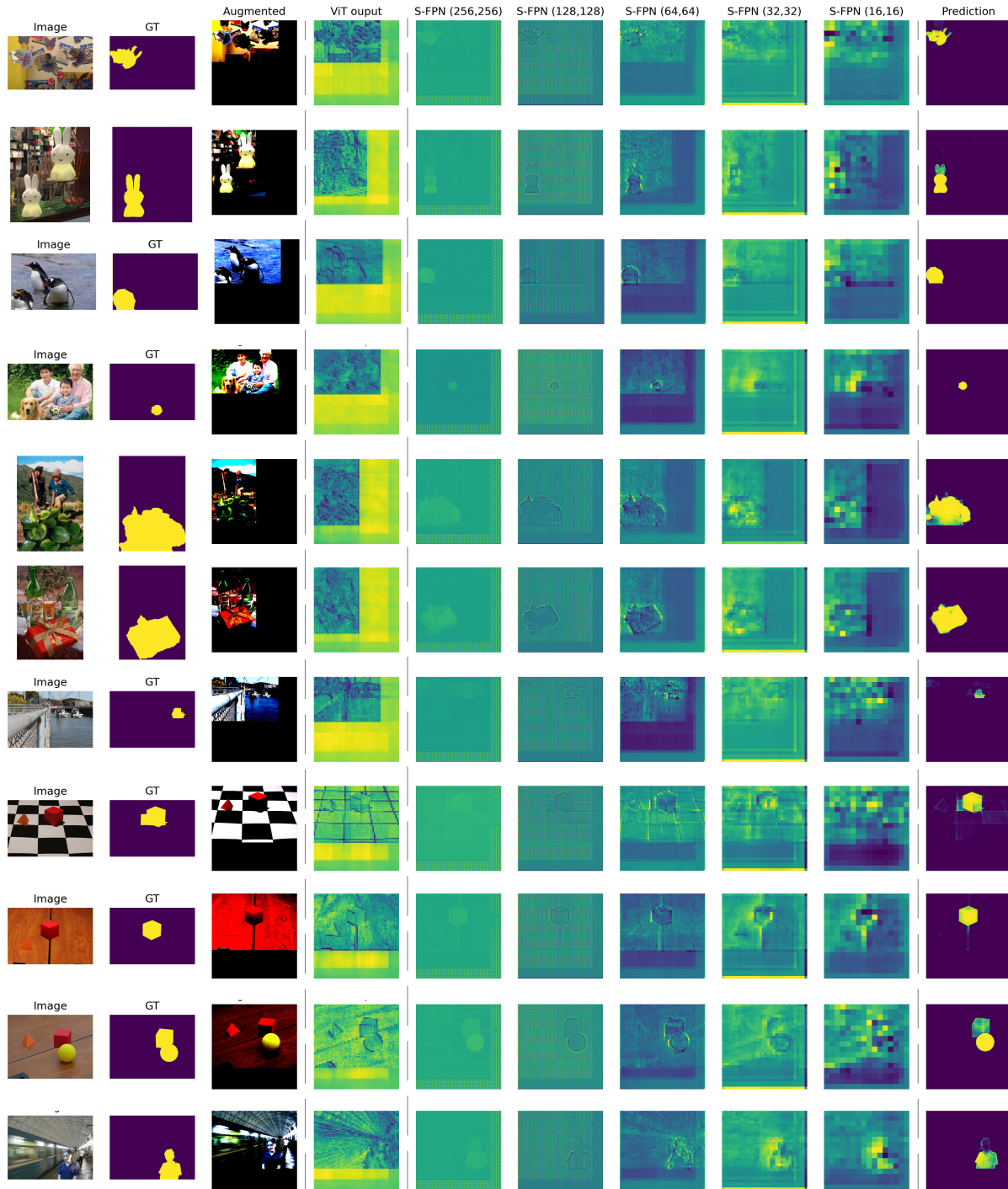


Figure 8: **Visualization of the outputs from each component.** *GT* denotes ground truth; *Augmented* refers to the image after padding and normalize; *ViT output* is the feature map for the output of ViT backbone; *S-FPN* denotes the respective output of each resolution for different outputs in *simple feature pyramid*. For the output of ViT, since visualization takes the average of all channels, we cannot effectively observe the discrepancies between the manipulated region and the authentic region. However, we are pleased to see different types of feature expressions in the multi-level output of *S-FPN*. In the high-resolution output, more representation is given to larger, region-level “contrast differences”, while in the (64×64) feature map, we see the image focusing more on edge details and artifacts. This result is in line with the design logic of IML-ViT, which tracks tampering detection from both the perspective of comparing regional low-level differences and capturing detailed visible traces, proving the rationality and effectiveness of our IML-ViT.